Journal of Biomedical Optics 9(1), 22–37 (January/February 2004)

Ocular static and dynamic light scattering: a noninvasive diagnostic tool for eye research and clinical practice

Rafat R. Ansari
National Aeronautics and Space Administration
Glenn Research Center at Lewis Field
Mail Stop 333-1
21000 Brookpark Road
Cleveland, Ohio 44135
E-mail: rafat.r.ansari@nasa.gov

Abstract. The noninvasive techniques of static and dynamic light scattering are emerging as valuable diagnostic tools for the early detection of ocular and systemic diseases. These include corneal abnormalities, pigmentary dispersion syndrome, glaucoma, cataract, diabetic vitreopathy, and possibly macular degeneration. Systemic conditions such as diabetes and possibly Alzheimer's disease can potentially be detected early via ocular tissues. The current state of development of these techniques for application to ophthalmic research and ultimately clinical practice is reviewed. [DOI: 10.1117/1.1626663]

Keywords: static light scattering; dynamic light scattering; cataract; age-related macular degeneration; diabetic retinopathy; Alzheimer's disease; ophthalmology; early detection; bioastronautics; telemedicine; ocular disease.

Paper 103017 received Apr. 18, 2003; revised manuscript received Jul. 25, 2003; accepted for publication Jul. 25, 2003.

1 Introduction

Blindness or serious vision impairment is one of the most feared disabilities known to humankind. A 2002 report[1] on vision problems in the United States compiled by the National Eye Institute (NEI) of the National Institutes of Health (NIH) and Prevent Blindness America states that although half of all blindness can be prevented, the number of people who suffer vision loss continues to increase. The American baby-boomer generation is aging and living longer than ever before. As a result, the rise of cataract, glaucoma, age-related macular degeneration (AMD), and diabetic retinopathy in the next two to three decades is expected to place a significant burden on the national economy. The personal cost of blindness is immeasurable, since no dollar value can be placed on the quality of human life. The problem is global in nature and not just confined to the United States. Malnutrition, lack of good surgical facilities, and inadequate hygienic conditions—for example the lack of clean drinking water in Africa and the Indian subcontinent—are some of the major factors contributing to vision problems. No medical treatments are available for the majority of ocular diseases, and most of the time surgical intervention is the only option (e.g., for cataract). Cataract is not only restricted to the aging population here on earth, it is also a risk factor for astronauts traveling and working in space, owing to radiation exposure.[2,3] The challenge is therefore to diagnose ocular diseases noninvasively long before the clinical symptoms appear and to help find nonsurgical countermeasures to prevent vision impairment.

The technique of dynamic light scattering (DLS) was developed by physicists in the late 1960s to early 1970s. Today, it is routinely used in laboratory settings to study fluid dispersions of colloidal ($\leqslant 1\ \mu$m) particles.[4] The pioneering work of Tanaka and Benedek in 1975 at MIT[5] introduced quasi-elastic light scattering (QELS) or DLS to the study of cataractogenesis, and Bursell and colleagues (1990)[6] gave an excellent review of DLS in the eye's anterior segment. I present here a review of new developments. DLS is now emerging as a potential ophthalmic tool, making possible studies of virtually every tissue and fluid comprising the eye, thus pushing the envelope for broader applications in ophthalmology.

New ocular DLS instrumentation is several orders of magnitude more sensitive than the current ophthalmic instruments of slit-lamp biomicroscopy (with and without retroillumination) and Scheimpflug systems. These conventional clinical instruments are based on imaging technologies and provide photographs of the various compartments of the eye. Other modern instruments, such as scanning laser ophthalmoscopes (SLO) and optical coherence tomography (OCT), provide high resolution (about few microns) and thus better-quality images. Although SLO and OCT are proving extremely valuable in the evaluation of retinal conditions, their use in other parts of the eye is yet to be established.

New DLS instruments are being used in clinical settings with better alignment and reproducibility to characterize the cornea, aqueous, lens, vitreous, and retina. Although they are still in the experimental realm, many new applications have been developed to detect a diverse range of diseases early, noninvasively, and quantitatively. These new applications include detection of pigmentary glaucoma, cataract, diabetic vitreopathy, and possibly Alzheimer's disease (via ocular tissues), as well as corneal evaluation after refractive surgery (e.g., laser-assisted *in situ* keratomileusis, LASIK). Recently, DLS has been used in conjunction with other complementary noninvasive techniques by integrating it with autofluorescence, Scheimpflug-based imaging, and corneal topography devices.

1083-3668/2004/$15.00 © 2004 SPIE

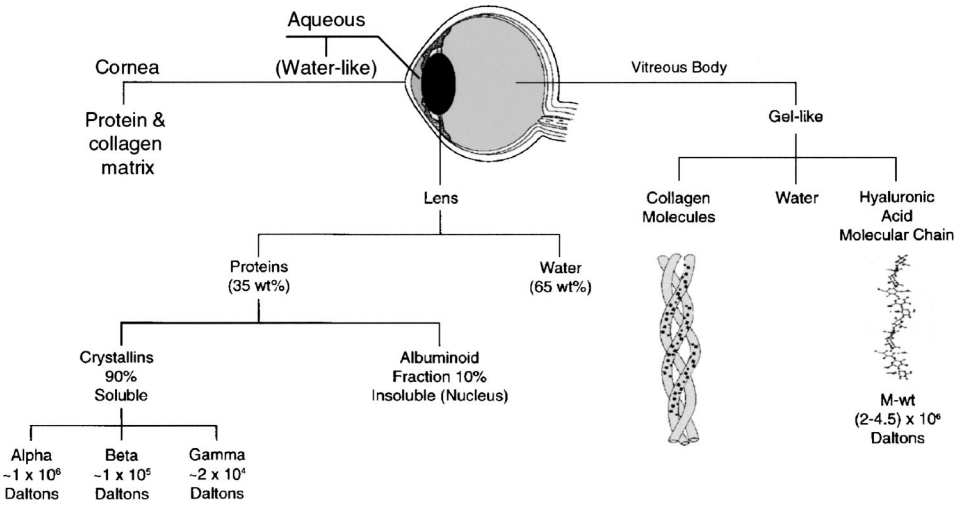

Fig. 1 Major ocular components of interest in a light-scattering experiment and their physical characteristics.

2 Principles Underlying Ocular Static Light Scattering and Dynamic Light Scattering

In general, light scattering occurs when a light beam interacts with a system of particles by excitation and reradiation of light. The electric field vector of the incident light can induce an electric dipole moment in a particle (excitation). This oscillating dipole, owing to a varying electric field, itself becomes a source of electromagnetic radiation (reradiation). This new radiation is the scattered radiation. Scattered light intensity is highly dependent upon the wavelength (λ) of the incident light and is inversely proportional to the wavelength.[5] This is known as Rayleigh's phenomenon and explains the blue color of sky, which is caused by the scattering of sunlight by earth's atmosphere.

For the present discussion and in the context of ophthalmic diagnostics, I divide light-scattering methods into two major categories: static and dynamic. Static methods are commonly used in the determination of weight-average molecular weight and the radius of gyration of macromolecules suspended in transparent solutions, while dynamic methods are used in the elucidation of diffusing behavior and the determination of the size and size distribution of these particles. The flow diagram in Fig. 1 shows the major structural components in the human eye and their macromolecular compositions and dimensions. When light impinges upon these macromolecules, they scatter light, depending upon their size and concentration. For example, α-crystallins in the lens contribute significantly to scattered light since they have a higher molecular weight. This and other macromolecular species of interest are discussed in the following sections.

2.1 *Static Light Scattering*

Static light scattering (SLS) simply consists of launching light into a system of scatterers and collecting the scattered light. In a transparent system such as pure water, the magnitude of the detected scattered intensity is virtually negligible since water molecules do not scatter light significantly because their molecular size is much smaller than the wavelengths of visible light. However, scattered light intensity increases significantly as the molecular size grows to the same order as the wavelength of the incident light. An increase in the amount of scattered light is an indication of a change in the morphology of the scatterers and therefore can be used to characterize a system qualitatively. This can be used to measure early morphological changes in the cornea, aqueous, lens, vitreous, and possibly retina.

An example of this is shown in Fig. 2 in which an eye of a 2-year-old guinea pig was scanned with a compact fiber optic probe, described later, that collects backscattered photons *in vivo*. The SLS scan clearly shows the anatomical features of the transparent eye in this animal. Based on the magnitude of the scattered light intensity, the corneal epithelium, stroma, and endothelium, as well as the lens (anterior-posterior) and vitreous are identified. Initially, the intensity rises rapidly at the cornea–air interface owing to a change in the refractive index. It decreases in the stroma and then increases in the endothelium. Local variation in intensity within the stromal structure can be attributed to the scattering of light from uniform collagen fibrils and fibroblasts that are interposed at equal distances.

2.2 *Dynamic Light Scattering*

The technique of dynamic light scattering provides a quantitative measure of early morphological changes by following

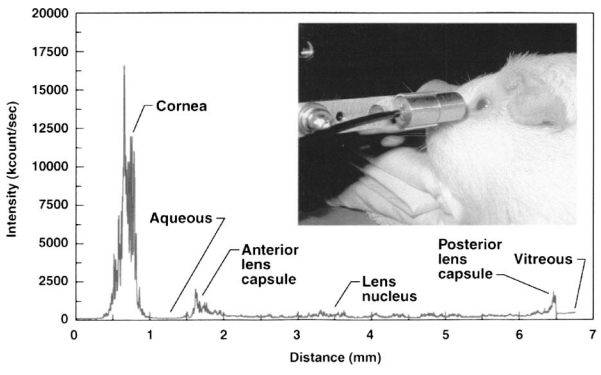

Fig. 2 Static light scattering (SLS) scan showing ocular anatomical features in a guinea pig.

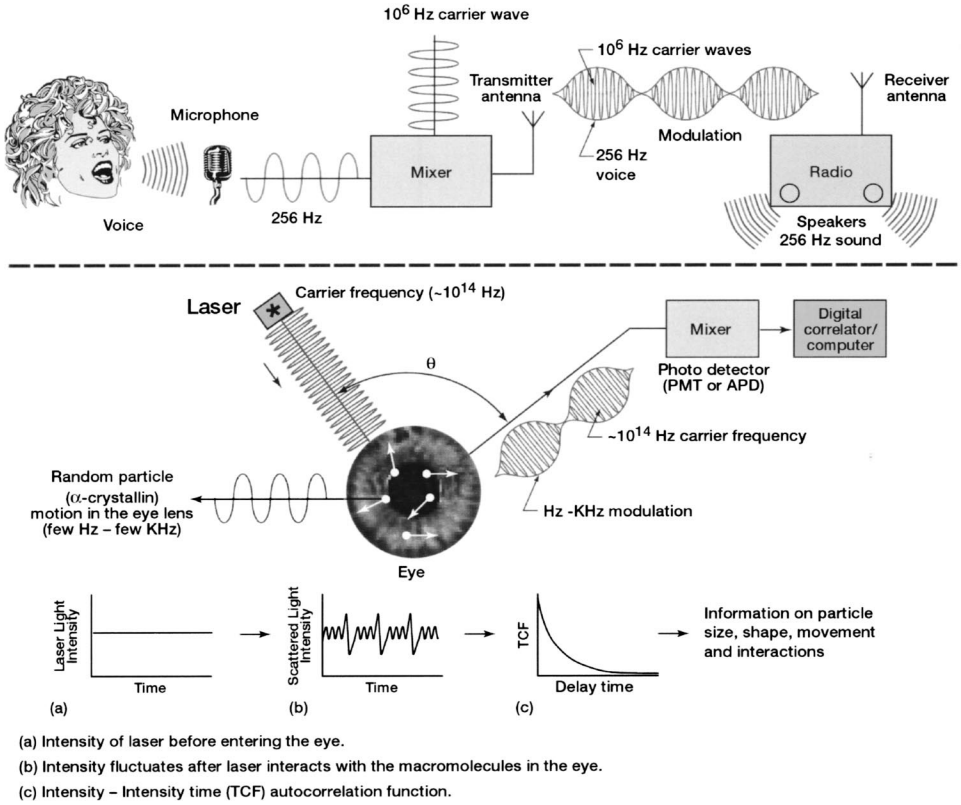

Fig. 3 Dynamic light scattering (DLS) in analogy with radio communication.

temporal changes in and around the random positions of scatterers as they undergo Brownian motion on a time scale of $\geqslant 1$ μs. Dynamic information such as diffusion, size, shape, molecular interactions, and flexing motion in polymers can be obtained. This makes DLS a unique tool for probing macromolecular dynamics.[4] The most attractive features of DLS are that it is noninvasive and quantitative, works effectively for particle sizes ranging from a few nanometers to a few micrometers, requires only a small sample volume, and works reasonably well for polydisperse or multiple-size (up to two to three component) dispersions. DLS is synonymous with quasi-elastic light scattering, photon correlation spectroscopy (PCS), light-beating spectroscopy (homodyne and heterodyne), and intensity fluctuation spectroscopy (IFS). These concepts were borrowed from the techniques used in radio communication.

Figure 3 is an oversimplified depiction of how a DLS measurement is performed in analogy to radio communication. In radio transmission, a microphone converts an audio (voice) signal with an approximate frequency of 256 Hz into electrical pulses. These pulses are then mixed (superimposed) with a carrier wave whose frequency is on the order of 10^6 Hz. This process is called frequency modulation (FM) or amplitude modulation (AM). The final AM or FM signal is then transmitted via an antenna into the atmosphere. On the receiver end, a radio antenna intercepts the transmitted signal, and if it is tuned to the same frequency as the transmitted signal, it decodes the desired audio signal. At this stage, the opposite of the transmission process takes place and the audio signal is decoupled from its carrier frequency. The desired information is recovered through a speaker diaphragm vibrating at the same audio frequency as the original voice signal.

In an analogous manner, the laser beam in a DLS measurement can be considered a carrier wave on which the particle (Brownian) motion is superimposed. The particles are often suspended in a fluid. The Brownian motion results from the collisions between the particles and the fluid molecules. On the receiver end (depending on the scattering angle θ) scattered light is collected, decoupled from the laser frequency, and dynamic information about the particles is obtained. This includes information on shape, size, movement, and the interactions among the particles, which can be of vital importance, e.g., in monitoring a cataract as it grows.

2.2.1 *Theoretical methodology*

In the absence of particle–particle interactions (dilute dispersions), light intensity scattered from small particles fluctuates rapidly, while light intensity scattered from large particles fluctuates more slowly. Assuming that the particles are uniformly sized and spherically shaped, in a simple homodyne experiment only scattered light intensity is collected (in the absence of a local oscillator) at a photodetector and an intensity-intensity temporal autocorrelation function (TCF) is determined.

$$g^2(\tau) = A[1 + \beta \exp(-2\Gamma\tau)], \tag{1}$$

where $A = \langle i \rangle^2$ is the average dc photocurrent or the baseline of the autocorrelation function, and β ($0 < \beta < 1$) is an empirical experimental constant and a measure of the spatial coher-

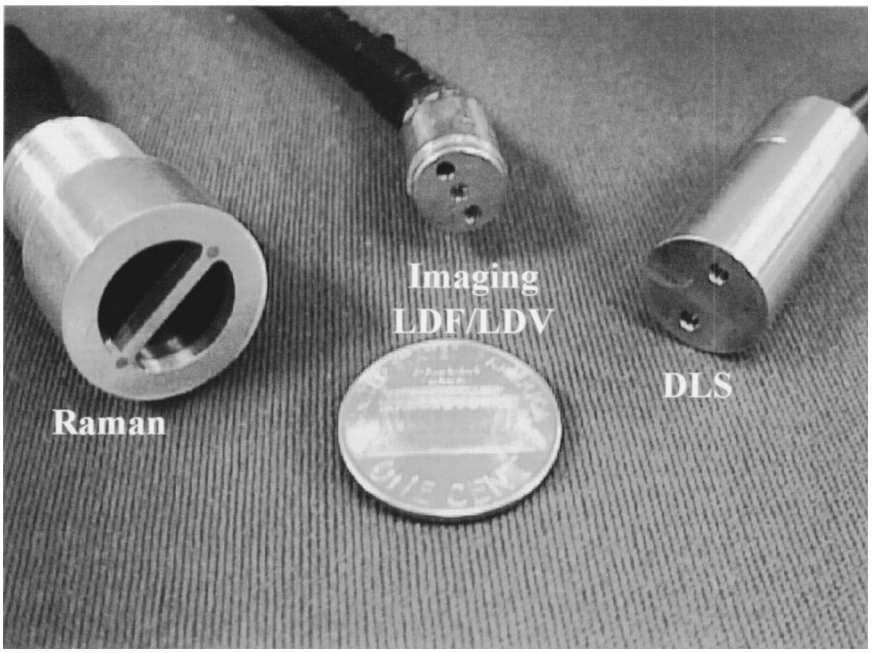

Fig. 4 Compact fiber optic probes.

ence of the scattering geometry of the collection optics which can be related to the signal-to-noise. (S/N) ratio. Γ is a decay constant that is due to diffusing motion of the particles in the scattering volume, and τ is the delay time.

$$\Gamma = D_T \times q^2, \tag{2}$$

where D_T is the translational diffusion coefficient and q is the magnitude of the scattering wave vector.

$$q = \frac{4\pi n}{\lambda} \sin\left(\frac{\theta}{2}\right), \tag{3}$$

where n is the refractive index of the solvent, λ is the wavelength of the incident light in a vacuum, and θ is the scattering angle. Using the Stokes-Einstein relationship for spherical particles, D_T can be related to the hydrodynamic radius (R) of the particle:

$$D_T = \frac{KT}{6\pi\eta R}, \tag{4}$$

where $K\,(1.38\times10^{-23}\,\mathrm{J\,K^{-1}})$ is Boltzmann's constant, T is the absolute temperature of the scattering medium, and η is the solvent's viscosity. In clinical ophthalmic applications, the values for water can be used for n and η at a temperature of 37°C (body temperature). Equation (4) then can be used to extract an average size of the particles in the transparent aqueous, lens, and vitreous. The lens and vitreous are polydisperse in nature and exhibit bimodal behavior. Today, commercial software packages are available to analyze Eq. (1) in terms of bimodal and multimodal size distributions based upon the schemes reviewed by Stock and Ray.[7]

3 Instrumentation

Until now, SLS and DLS instruments were bulky, required vibration isolation, indexmatching (for flare control), and tedious optical alignment, and were difficult to use. Thanks to several key advances in the field of optoelectronics technology in the past decade, DLS can now be safely used in clinical ophthalmic settings. New-generation DLS systems have become very compact and efficient as a result of new solid-state laser sources, sensitive photodetectors, and monomode optical fibers for launching (and detecting) low levels of laser light into the eye.

3.1 *Compact SLS-DLS Fiber Optic Probes*

The fiber optic-based DLS design developments for studies of cataractogenesis are covered by Dhadwal et al.,[8] Rovati et al.,[9] Ansari et al.,[10] and the references contained in their papers. The fiber optic SLS-DLS probes, shown in Fig. 4 and diagrammed in Fig. 5, combine the unique attributes of small

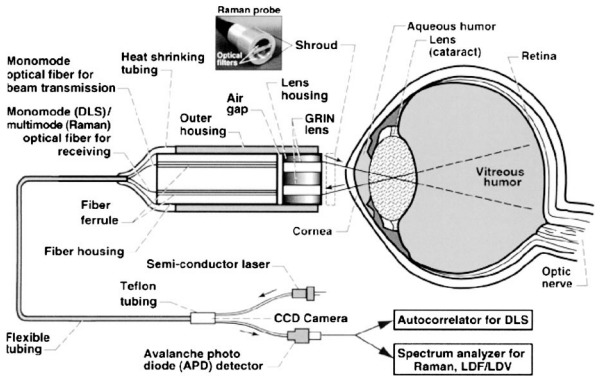

Fig. 5 Schematic of probe.

size and low laser power with high sensitivity [the β values in Eq. (1)]. They were originally developed to conduct fluid physics experiments under the challenging conditions of microgravity on board a space shuttle or space station orbiter. This type of probe is easy to use because it requires neither precise optical alignment nor vibration isolation devices. Currently it has been successfully employed in many ocular experiments to detect early effects of various eye diseases. A low-power (50 to 100 μW) light from a semiconductor laser, interfaced with a monomode optical fiber, is tightly focused on a 20-μm diameter focal point in the tissue of interest via a graded refractive index (GRIN) lens. On the detection side, the scattered light is collected through another GRIN lens and guided onto an avalanche photodiode (APD) detector built into a photon-counting module. APD-processed signals are then passed onto a digital correlator for analysis. The probe provides quantitative measurements of pathologies in the cornea, aqueous, lens, vitreous, and retina. The device is modular in design. If needed, by a suitable choice of optical filters it can be converted into a device for spectral measurements (autofluorescence and Raman spectroscopy) and laser Doppler flowmetry or velocimetry, providing measurements of molecular structure and blood flow in the ocular tissues. The device can be easily mounted onto many conventional ophthalmic instruments to significantly increase their diagnostic power.

3.2 *Sensitivity of DLS Over Established Clinical Technologies in the Early Detection of Cataract*

The gold standard in the evaluation of cataract is still slit-lamp biomicroscopy and/or Scheimpflug photography using various clinical grading standards of lens opacity, such as the lens opacity classification system (LOCS), Oxford, Wilmer, or Wisconsin systems. The interpretation of photographs using these grading systems remains subjective. Recent clinical studies using DLS were reported by Thurston et al.,[11] Rovati et al.,[9] Dhadwal and Wittpen,[12] and Datiles et al.,[13] and the references contained in their publications.

DLS has been found to be far superior in detecting cataract changes very early in the natural history of the disease. But until recently it was not demonstrated just how early a cataract can be detected in a quantitative manner. This was resolved by comparing DLS and Scheimpflug imaging (SI) techniques simultaneously. A detailed description of the SI technique is given elsewhere.[14] The SI technique provides a measure of lens opacity by converting stereoscopic lens images into a turbidity parameter expressed in optical density units (ODU).[14] An ODU value of 0.01 represents the transparency of an ultraclean sample of water. Clinically, a range of values $<$0.1 ODU is assigned to a normal (noncataractous) lens.

The DLS fiber optic probe described earlier was mounted on an SI system for an objective study of lens opacity.[14] The instrument's sensitivity was evaluated by slowly inducing a nuclear cold cataract in a calf eye, taking Scheimpflug photographs and DLS data simultaneously (within a few seconds of each other). The γ-crystallins also known as cryo (low-temperature) proteins in a calf lens promote the aggregation of α-crystallins, causing lens opacity as the temperature is lowered. The Scheimpflug images and the DLS data are compared in Fig. 6. The protein particle size distributions consistently shifted from left to right in the direction of increasing sizes at each temperature decline, from 18°C down to 9°C. This can be attributed to the formation of protein aggregates and high molecular weight complexes even though the lens remains transparent. Scheimpflug images, however, did not detect any change until 10°C, when the optical density increased from 0.01 to 0.02 ODU. This value corresponds to N0 on the LOCS-II clinical cataract grading system. The grading ranges from N0 (no cataract) to N4 (mature cataract). The equivalent ODU values are approximately 0.050 (N0), 0.09 (N1), 0.21 (N2), 0.46 (N3), and 0.56 (N4).

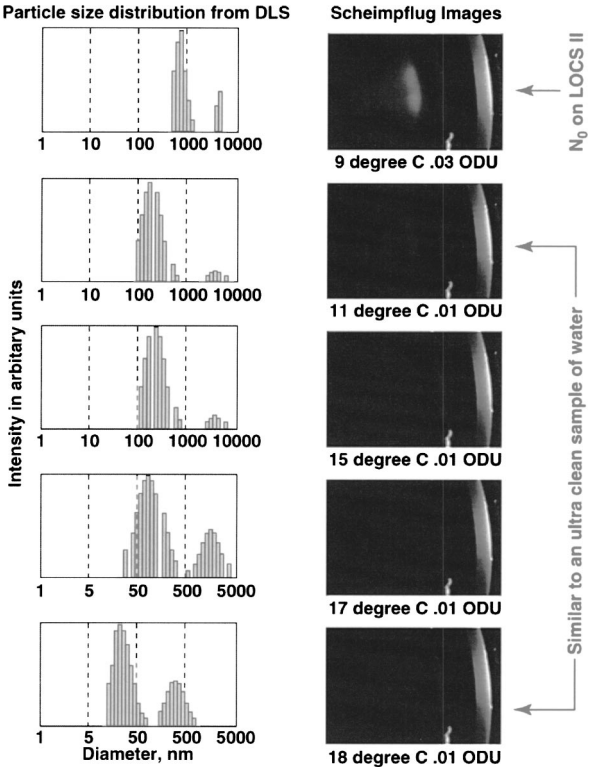

Fig. 6 Scheimpflug images and DLS size distributions.

One symptom of a developing cataract is glare that is due to increased light scattering. DLS data complement SLS data, as shown in Fig. 7. The scattered light intensity increases as a

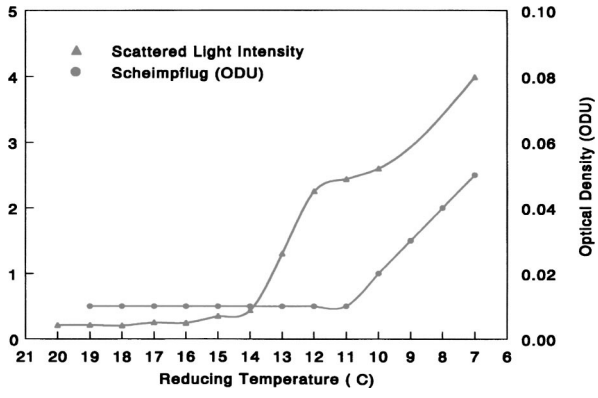

Fig. 7 Comparison of Scheimpflug optical density units (ODU) and DLS scattered light intensity.

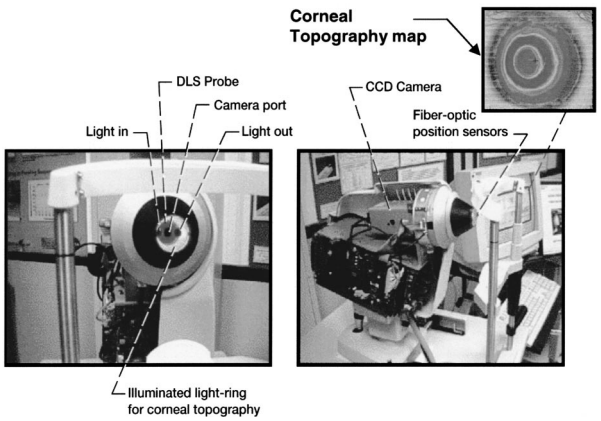

Fig. 8 Front and cutaway view of a modified corneal analyzer (Keratron) with a DLS probe.

function of decreasing temperature. This intensity increases slowly at first, with a sharp increase at 14°C, and continues increasing as the temperature continues to drop. In contrast, the ODU from Scheimpflug remains constant until 10°C. At 7°C, ODU measurements increased to 0.06 (error limit: $\pm$0.023 ODU),[14] which corresponds to N0 (normal) on the LOCS-II grading scale. Based on these dynamic and static observations, it can be concluded that DLS is 2 to 3 orders of magnitude more sensitive than the SI imaging system for detecting cataract early.

3.2.2 *New clinical DLS instrumentation for ophthalmic diagnostics*

Until recently, almost all DLS instruments have employed slit-lamp biomicroscopy in one way or another[8,11] because of its familiarity to ophthalmologists. In our earlier work, we simply mounted the DLS probe discussed earlier on a slit-lamp biomicroscope using a Hruby lens holder. Conceptually, these setups were easy to use and provided ease of alignment, since a test site for DLS measurement was selected by directly observing the lens with the view that ''you measure what you see.'' However, their ability to sample the same location in the lens repeatedly and reliably is questionable. It is very important to sample from the same location because the lens is not homogeneous and a slight misalignment can give erroneous results, especially in repeat patient visits during longitudinal studies. New instruments have been developed to circumvent these problems by combining DLS with other ophthalmic instruments employing such technologies as autofluorescence and keratoscopy. The advantage of this is that not only can the sampling issue be resolved but DLS data can also be compared with other complementary ocular data, e.g., oxidative stress, as shown in the review article on autofluorescence by Rovati and Docchio in this issue.

A corneal analyzer (Optikon 2000 Keratron, Italy) utilizes an infrared (IR) detector that pinpoints the exact location of the corneal vertex. The front-end eyepiece is equipped with two fiber optic position sensors on the extreme (equatorial) ends. An IR beam passes through one fiber and is collected by another fiber at the opposite end. When this beam is intercepted by the cornea (see Fig. 8 and Fig. 9), the instrument is aligned with the apex of the cornea. This instrument was modified by placing a DLS fiber optic imaging probe inside its cone as shown in Fig. 8 and Fig. 9. The DLS portion of the instrument takes measurements from the cornea to the retina by moving the DLS probe inside the cone using computer-controlled linear microactuators. Since the IR beam does not pass through any other ocular tissue, the actual laser light used during the 2 to 5-s DLS measurement is never used to align the instrument, as was the case in previous slit-lamp-based DLS instruments. This arrangement makes it much safer for human use. During the DLS measurement, the subject is asked to fixate on a light source housed inside the cone and probe assembly.

Using the CCD camera located in the center of the cone (Fig. 9), an operator uses a joystick to center the cone with the optical axis of the eye, in order to view the active image of the patient's eye on the instrument's built-in CRT screen, as

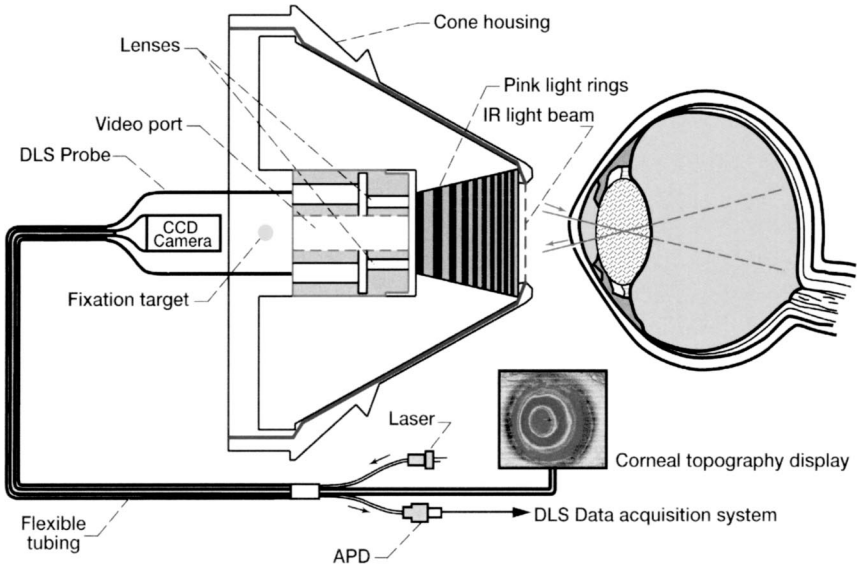

Fig. 9 Schematic diagram of the optical system.

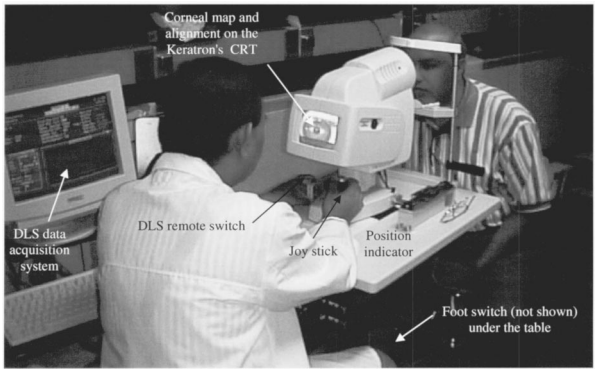

Fig. 10 Instrument in clinical operation.

shown in Fig. 10. When the foot switch is depressed, the IR detection system automatically sends a signal to the computer, instantaneously grabbing the image when the desired position of the cone has been achieved. The operator simultaneously depresses the ''remote DLS'' button, which in turn activates the laser and starts the digital autocorrelator for the DLS measurement. The patient sees a diffused speckle light pattern during the 2 to 5-s DLS measurement. The laser and the data acquisition program can be preset to run for either a 2-s (for the cornea) or a 5-s (for the lens) measurement time. The operation sequence is shown in Fig. 11.

This new instrument has demonstrated its reproducibility and ability to go back to the same location in the lens during repeat patient visits.[13] Since that study, about 50 patients have been studied at the National Eye Institute in Bethesda, Maryland. None reported any discomfort during or after the DLS measurements. The data will be useful in planning a longitudinal study of anticataract drug(s) screening at the NEI.

4 Applications to Ophthalmic Research

4.1 *Cornea*

Corneal tissue is avascular and composed primarily of collagen. The human cornea is about 500 μm thick at the apex and about 700 μm at the periphery or limbus.[15] Transparency is the most important corneal property in maintaining good-quality vision. A slight loss of transparency can cause problems such as haze and glare. Histologically the cornea is structured as a stack of layers divided into five distinct regions. These include the epithelial cell layer, Bowman's layer, stromal layer, Descemet's membrane, and the endothelial cell layer. The epithelial layer (about 50 μm thick) consists of six to eight layers of cells of which two to three layers are superficial flat cells, followed by a squamous, irregularly shaped wing (about two layers), and a single layer of cylindrical basal cells. Bowman's membrane (about 10 μm thick) is a dense, irregular meshwork of interwoven collagen fibrils of type I and type VII without a cellular structure (no fibroblasts). The stromal layer comprises 90% of the thickness and volume of the cornea, consisting of uniform-diameter collagen fibrils (about 200 in number) with regular spacing. Fibroblasts are interposed in these collagen layers. Descemet's membrane is a tough, glassy layer that can vary in thickness from about 5 to 15 μm as a function of age. The endothelium consists of a single layer of metabolically active, irregular polygon-shaped cells about 20 μm in diameter.[15] The tear film (about 7 μm thick) on the surface of the epithelium prevents the cornea from dehydrating.

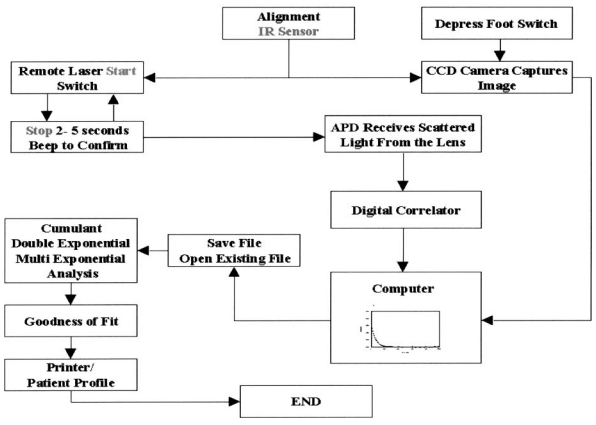

Fig. 11 Block diagram of data acquisition and analysis.

The use of SLS and DLS in the cornea offers opportunities and challenges. The opportunity lies in its transparency, since the normal cornea does not exhibit multiple scattering of light. However, at first glance, the different layers and structures within the cornea seem very challenging when one is interpreting DLS data. Furthermore, corneal tissue is far from the ideal case of a dispersion containing colloidal particles. One should therefore refrain from interpreting corneal DLS data in terms of particle size because of many unknown quantities (local viscosity, refractive index, etc.). However, it is reasonable to report the decay constant Γ (s^{-1}) from Eq. (1), which represents the time relaxation values of a scatterer as it executes limited Brownian excursions about fixed average positions in the corneal tissue.

4.1.1 *Brownian spectrum of the cornea*

As described in Sec. 2.2.1, the construction of a TCF [Eq. (1)] in a DLS experiment relies heavily on measuring the fluctuations of scattered light intensity in a time domain. To demonstrate this point, an experiment was performed on a model system of polystyrene microspheres in the size range of 70 nm to 1 μm suspended in water, and the time fluctuations were compared with the scattered light intensity as a function of particle size. The spectrum of the microspheres is illustrated in Fig. 12(a), for 70-nm, 250-nm, and 1.05-μm particles. As expected, the time fluctuations in this freely diffusing system of particles gradually slow down as the particle size increases. The time decay constant (Γ) shown in Fig. 12(b), which was obtained directly from the TCF, further illustrates this point. It shows that small particles move very fast while larger particles move very slowly and in a random fashion around their fixed average positions. Thus, Γ becomes a powerful parameter when one is characterizing a system of freely diffusing and bound particles without prior knowledge about the system (e.g., viscosity, refractive index, size).

Figure 13 compares the intensity fluctuations within the layers of a normal bovine cornea in an intact eye, *in vitro*. The components in the anterior stroma fluctuate slowly, while in the middle and posterior sections the fluctuations are relatively faster. The endothelial cells fluctuate much more

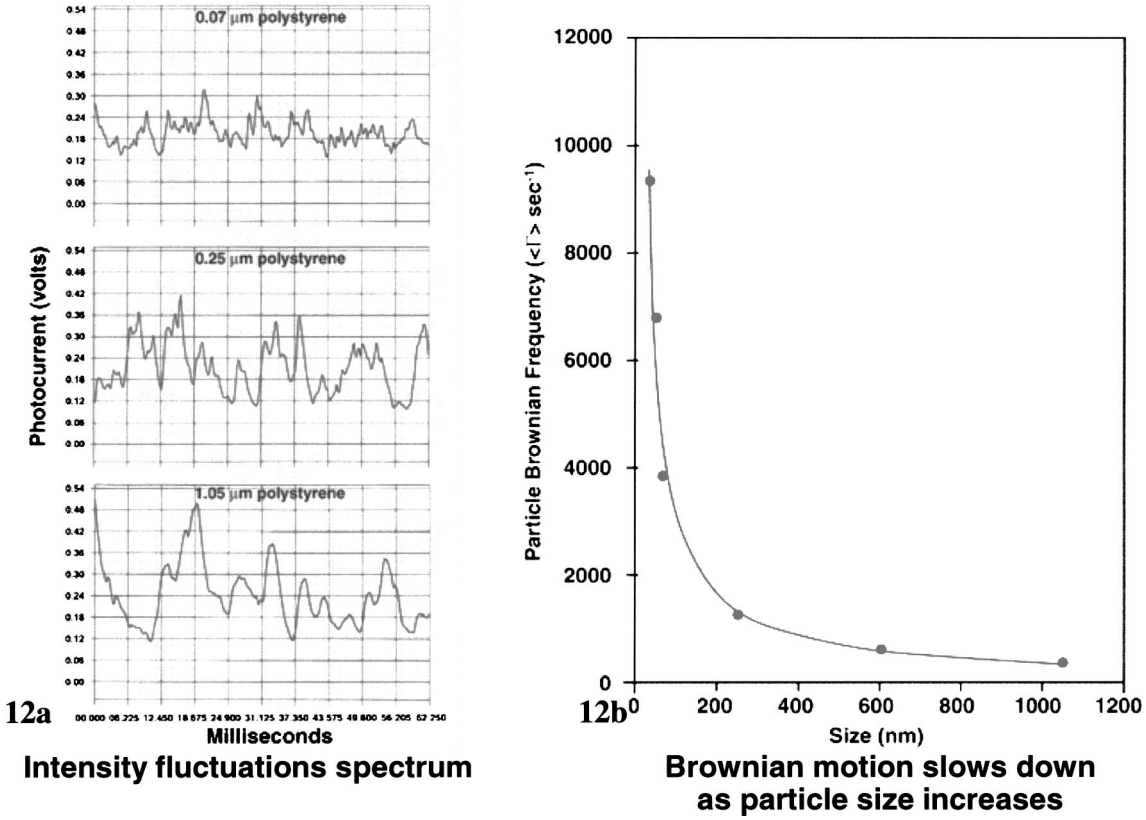

Fig. 12 (a) Intensity fluctuations and (b) Brownian motion.

slowly. When the laser light enters the anterior chamber, the fluctuations almost disappear. Thus we can infer that either the clear aqueous humor in the bovine eye contains hardly any particles or proteins of a size to scatter light or the power level of the probing laser light of (a few microwatts) is too low, resulting in the intensity of scattered light being too low to be detected. In either case, the power level of the scattered light is too low to construct a TCF or a spectrum. However, as described later, protein concentration in the human aqueous can increase during uveitis.

The polygon-shaped cells in the endothelium layer are rigidly bound and act like a reflecting mirror. As a result, the entire structure exhibits very slow Brownian motion. The faster fluctuations in the middle and posterior stroma can be attributed to the presence of protein particles and an increased amount of water. Indeed, the water content increases from the anterior to the posterior cornea, as shown by Castoro et al.,[16] using differential scanning calorimetry. This may be why the fluctuations in the anterior stroma are relatively slower. In terms of post-LASIK complications, since the epithelium layer is preserved in a flap, the stromal region can be of prime interest for examination with DLS.

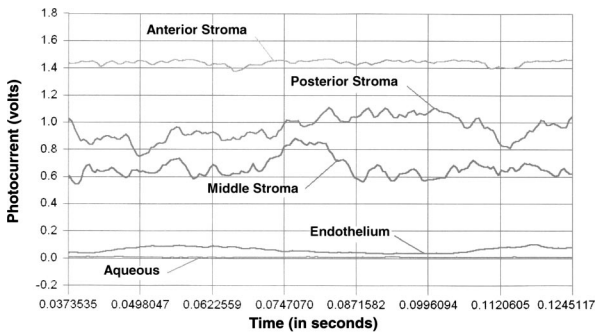

Fig. 13 Brownian spectrum of bovine cornea.

4.1.2 *Evaluation of corneal abnormalities*

A change in the physical shape of the cornea can lead to ametropia (myopia, hyperopia, or astigmatism). Thus modern photorefractive surgeries, such as LASIK, have become popular in treating corneal refractive errors. The goal of refractive surgery is to sculpt the corneal surface, changing its physical shape. If successful, it will result in the elimination of overall refractive errors. In about 5% of post-LASIK cases, patients experience a variety of problems, such as haze, glare, star bursts, dry-eye syndrome, and tissue healing issues. Lipner[17] reported dry eye to be LASIK's most common complication, appearing, according to some statistics, in more than half of the cases performed in the United States. At present, no objective methods are available to evaluate quantitatively and noninvasively the underlying molecular changes causing these corneal abnormalities after a LASIK procedure. McLeod[18] stressed the need for new diagnostic capabilities to better evaluate current refractive surgery outcomes.

Recently the SLS and DLS concepts discussed here were applied by Ansari et al.[19] to the study of the cornea as a way to develop a molecular measure of clarity. In a preliminary

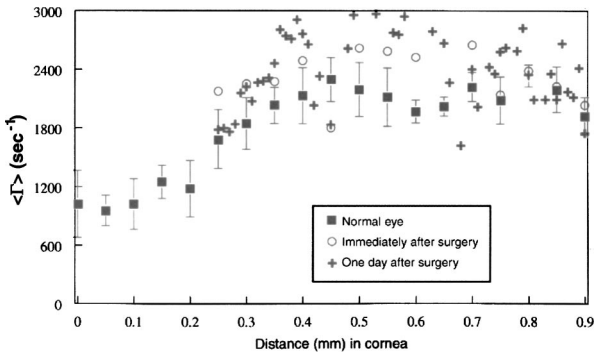

Fig. 14 Eye 1, photorefractive radial keratectomy (PRK), about 8 mm.

study,[20] intact bovine eyes were treated with chemicals, cotton swabs, and radial and photorefractive surgeries *in vitro*, and SLS-DLS measurements were performed as a function of the penetration depth into the corneal tissue. Topographical maps of corneal refractive power from untreated and treated corneas were also obtained using videokeratoscopy and the results compared.

4.1.3 *Post-LASIK results*

Two sets of DLS data are presented after LASIK surgery was attempted on two bovine eyes *in vitro*. Ronald Krueger, M.D. of the Cleveland Clinic performed these procedures. They are referred to as eye 1 (photorefractive radial keratectomy, PRK) and eye 2 (lamellar keratectomy, LK) and are shown in Fig. 14 and Fig. 15, respectively. The DLS measurements on the untreated cornea were repeated five times to get an estimate of variation (see error bars) in Γ values. The bovine corneas were found to be much more ''rigid'' than the human corneas, so an attempt to make a flap using a lamellar keratectomy of about 3 nm was not successful. In eye 1 the epithelium was scraped and the PRK procedure (about 8 mm in size, 5.5 diopters) was performed. In eye 2 the epithelium was scraped and two lamellar karatectomies about 5 mm (no laser ablation) with a residual thickness of about 720 μm were performed. Since the corneas are reduced in size after the surgery, the DLS data for treated corneas begin at a distance of 0.2 and 0.25 mm, respectively. The two surgically treated corneas show higher Γ values than their untreated counterparts. The PRK and LK results differ significantly. The PRK shows less increase in Γ values than the LK. This is perhaps due to the loss of water during the ablation process in the case of PRK. Since no laser ablation was performed in LK, the Γ values remain higher. It is of interest to note that for the most part, Γ values revert back close to untreated levels 1 day after surgery.

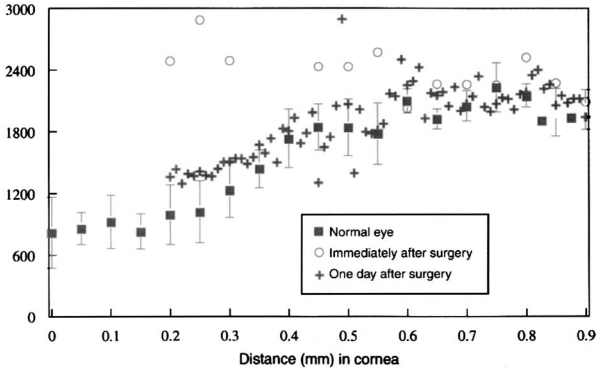

Fig. 15 Eye 2, lamellar keratectomy (LK), about 5 mm.

The eyes were kept in a jar of saline solution and refrigerated overnight after the surgeries. The LK procedure showed faster ''healing'' (return to baseline levels) than the PRK. After corneal injury, as in surgery, the area where the epithelium has been removed is reepithelialized by the sliding movement of the expanded remaining epithelium. Two factors affecting this healing process are the size of the denuded area and the smoothness of the denuded surface, as well as the presence or absence of cellular and other debris on the surface. The larger the denuded surface, the longer it takes to reepithelialize. Since the LK surface was only 5 mm, compared with the PRK (8 mm), it healed faster. The laser-ablated (PRK) surface will still have significant debris on the surface, whereas there will be almost no debris on the lamellar keratectomized surface (LK); this difference might explain why there seems to be more healing in the LK-treated cornea. These differences can be seen by the more rapid return to normal, baseline levels of the Γ values in the LK-treated cornea 1 day after the injury, compared with the PRK-treated cornea. However, more studies need to be performed to confirm these observations, such as using live animal models to follow the healing process using vital stains after LK scraping of the epithelium. The treatments discussed here also changed the corneal refractive power.

The results of these experiments suggested the potential of SLS and DLS in measuring changes in pre- and postrefractive surgeries. However, the actual feasibility of using the DLS technique diagnosis and treatment for clinical in early evaluation of corneal complications after LASIK surgeries and other corneal abnormalities has yet to be proven. At the time of this writing, this validation work is being conducted at NEI/NIH.

4.2 *Aqueous, Uveitis, and Glaucoma*

Aqueous humor can be considered an ultrafiltrate of blood since it contains most of the molecules found in serum at concentrations that are reflective of serum levels. For example, certain metabolites (glucose) and proteins (human serum albumin, HSA) are always present in the aqueous. Since glucose molecules are much smaller than the wavelength of light, they do not contribute significantly to scattered light. Because HSA particles can scatter light appreciably, since they are spherical in shape and their size (about a few nanometers) is comparable to the wavelength of light, they are frequently used in DLS experiments. Uveitis is an inflammatory disease of the eye. When the anterior chamber is involved, uveitis can produce high numbers of protein particles in the aqueous humor. This increase in protein concentration gives rise to increased scattered light intensity or ''flare'' in slit-lamp biomicroscopy. Clinically, flare and therefore the severity of uveitis, can be easily detected and quantified by SLS and DLS. Similarly, cholesterol levels in the body can also be evaluated through the aqueous, as suggested by Bursell.[6] This important application has not been pursued thoroughly, either in laboratory or clinical settings.

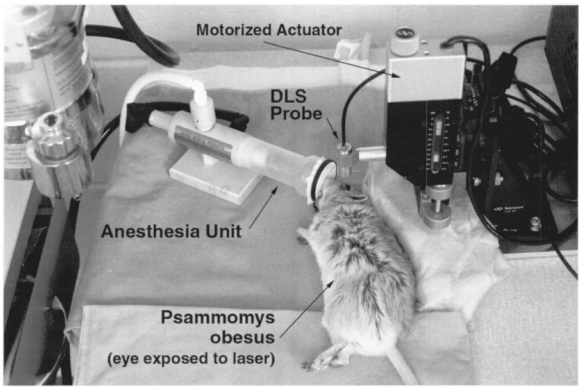

Fig. 16 SLS-DLS scanning setup for small animals.

Glaucoma is a disease in which the intraocular pressure (IOP) is often increased. If IOP increases are not treated, they can lead to degeneration of the optic nerve and eventually loss of vision. Recently, DLS was used to study one specific type of glaucoma known as pigmentary dispersion glaucoma (PDG). The posterior layer of the iris epithelium contains many melanin granules. These granules are released into the aqueous as a consequence of natural epithelial cell death, infection, or trauma. Excess melanin release into the aqueous occurs in patients with PDG. The melanin granules can be trapped in the trabecular meshwork, over time blocking aqueous outflow and causing an increase in IOP. Pollonini et al.[21] used DLS to detect and quantify aqueous melanin granules in a clinical study of normal and PDG volunteer patients. The results indicated the presence in the aqueous of small particles (1 to 10 nm) in normal patients and large particles (up to 1 μm) in PDG patients and therefore showed the potential of DLS in monitoring this type of glaucoma noninvasively.

4.3 *Lens and Cataract*

Cataract (lens opacification), its clinical evaluation, and its classification is discussed in detail elsewhere by Datiles and Ansari.[22] Snellen acuity charts, contrast sensitivity tests, visual function questionnaires, examinations with direct ophthalmoscopes, slit-lamp biomicroscopy, Scheimpflug imaging, and retroillumination imaging techniques are routinely employed in cataract evaluation. However, these methods fail to detect and grade cataracts reliably and quantitatively at their early stages of formation. The validation of DLS techniques in animal models is a logical first step before human trials.

4.3.1 *Cataractogenesis in small animal models*

Animal models are usually helpful in the validation of new instruments and testing of therapies prior to clinical use. Until recently, it was difficult to use SLS and DLS in small animals (e.g., mice) mainly owing to instrument limitations (e.g., physical size, power requirements, and alignment problems). Compact DLS probes developed at the National Aeronautics and Space Administration (NASA) and shown in Fig. 4 are proving to be very useful in this area of research. A generic experimental setup is shown in Fig. 16. Cataractogenesis is monitored *in vivo* by following TCF profiles [Eq. (1)] on different time lines. As an example, Auto-Correlation Profiles for Philly mice are shown in Fig. 17(a). This animal develops cataract spontaneously between days 26 and 33 after birth. The data include a 45-day-old normal mouse of the control FVB/N strain, which does not develop a cataract, and two Philly mice roughly 26 to 29 days old.

Examinations of these mice with a slit-lamp biomicroscope identified one normal (transparent) eye and two other eyes with trace cataracts. These examinations were conducted soon (within few minutes) after the DLS measurements were completed. Each measurement took 5 s at a laser power of 50 μW. The changing TCF slope is an indication of cataractogenesis as the lens crystallins aggregate to form high-molecular-weight clumps and complexes. The DLS autocorrelation data are converted into particle size distributions [Figs. 17(b) to 17(d)] using an exponential sampling program. Although conversion of the DLS data into particle size distributions requires certain assumptions regarding the viscosity of the lens fluid, these size values do indicate an increasing trend as the cataract progresses. These measurements suggest that a developing cataract can be monitored quantitatively with reasonable reliability, reproducibility (5 to 10%), and accuracy.

4.3.2 *Off-axis early cataract mapping*

Light falling on the cornea is guided by the pupil along the optical axis of the eye and is focused on the fovea by the lens. Any lens abnormality along this optical path, whether capsular, nuclear, or cortical, can potentially deteriorate the sharp focus of the image on the retina and thus vision. Therefore every DLS study of cataract has been carried out along the optical axis of the eye. Until recently, no DLS data were available for the peripheral regions of the lens. There is a debate among cataract researchers regarding the causes of subcapsular cataracts, nuclear cataracts, and cataracts occurring in the peripheral regions of the lens. Thus there is a need to gather data on the early onset of opacities simultaneously in different regions of the lens.

Ansari et al.[23] used DLS *in vivo* to map the lenses of HIV-1 protease transgenic mice to study early onset of cataractogenesis. Topographical colored contour maps (cataractograms) were obtained noninvasively by automated scanning of the eye with a DLS probe in three dimensions (x, y, and z directions). Various colors in the map represent varying crystallin size and provide quantitative detection and monitoring of opacities in the entire lens. The portion of the lens mapped is, however, limited by the degree of pupil dilation ($\sim$1 mm) for the mouse eye. Four representative cataractograms are presented in Fig. 18 for transgenic mice ranging in age from 17 to 23 days. These images in false color (black to white) provide topographical contour maps of the lens that show the degree of severity of a progressing cataract. The cataractograms show a tiny amount of opacity developing on day 17, a small opacity occurring in the posterior region on day 22, and a dramatic increase on day 23, becoming large by spreading into nuclear and anterior segments of the lens. It is also interesting to note the change in the average scattered intensity as a function of increasing particle size. The average size changed from a minimum of 30 nm to 662 nm and intensity changed from 100 kilocounts/s to 1500 kilocounts/s. The average particle size increased 20-fold and the scattered light intensity increases 15-fold from day 17 to day 23. However, the normal strain does not develop a cataract, as shown for an 18-day-old normal mouse.

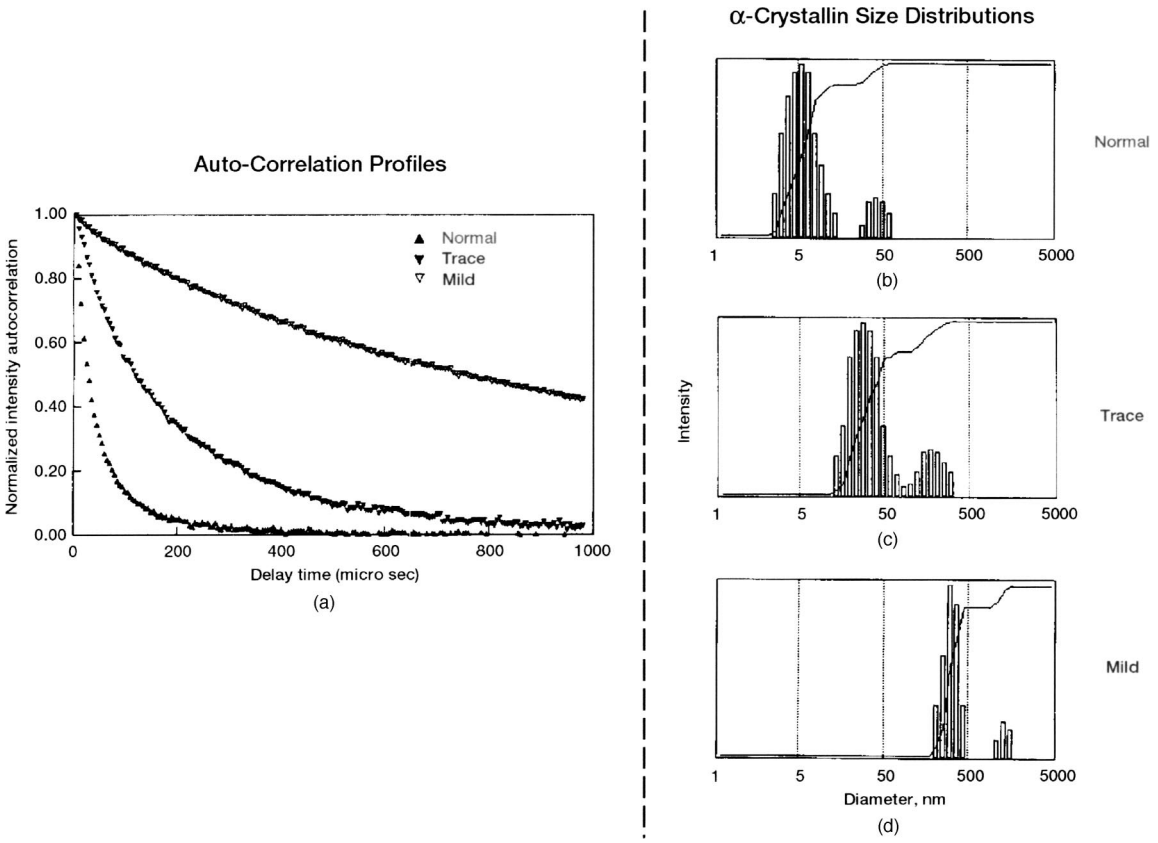

Fig. 17 *In vivo* cataract measurements in Philly mice. (a) Autocorrelation profiles. (b) Normal particle size distribution, control mouse. (c) Particle size distribution for a mouse with trace cataract. (d) Particle size distribution for a mouse with mild cataract.

The behavior we see here is very different from the formation of large protein complexes during the progression of a nuclear cataract, in which the particle size or intensity is expected to increase only in the central portion of the lens. In a study of HIV-1 protease transgenic mice, Tumminia et al.[24] found that cataracts appear between 24 and 26 days after birth. Bettelheim et al.[25] viewed hydration as a main cause of cataract formation in these animals, based on differential scanning calorimetry and thermogravimetric analysis. It is therefore clear that different mechanisms can be responsible for the formation of cataracts in humans and other animals. In summary, DLS was able to identify a progressing cataract under these widely different and distinct mechanisms of formation.

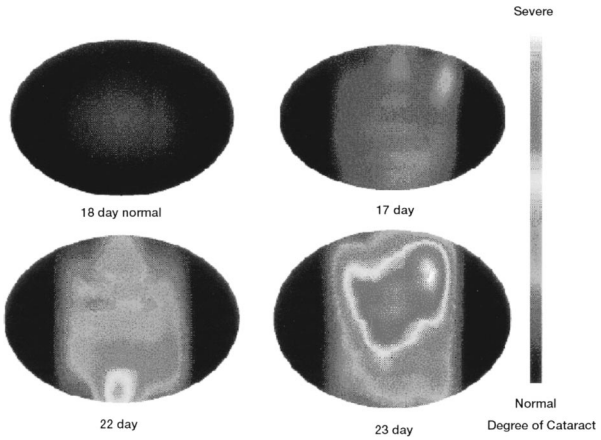

Fig. 18 Cataractograms (cataract mapping).

4.3.3 *Human congenital cataract*

As mentioned earlier, the present cataract grading systems are only applicable to age-related or senile cataracts and are thus not useful for congenital cataracts. Congenital or infantile cataract is a lens opacity that is present at birth. These types of cataracts are classified by their morphology, presumed etiology, the presence of certain metabolic disorders, or associated ocular or systemic findings.[26] The ability of DLS to study such opacities quantitatively in humans is discussed here. Figure 19(a) shows a slit-lamp photograph of the right eye of a 37-year-old male with a mild congenital nuclear cataract. It is located in the embryonic nucleus slightly off of the optical axis. The left eye of this volunteer patient was found to be transparent. The DLS measurements were taken about 6 mm from the cornea into the lens, both on and off the ocular optical axis. The particle size distributions plotted in Fig. 19(b) clearly show the presence of smaller protein particles in the clear section of the nucleus and aggregates of much larger particles near the visual opacity. The size distribution for the left eye is comparable to that of the right eye in the nucleus and is consistent with age-related changes for a similar age group.

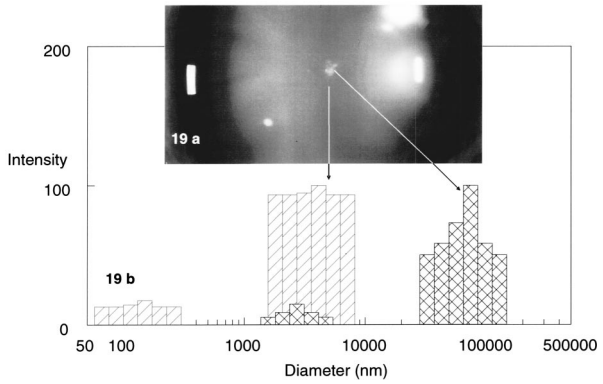

Fig. 19 Human congenital cataract. (a) Slit-lamp photograph. (b) Particle size distributions obtained by DLS. (See text for explanation.) (Slit-lamp photograph courtesy of M. B. Datiles, National Eye Institute/National Institutes of Health.)

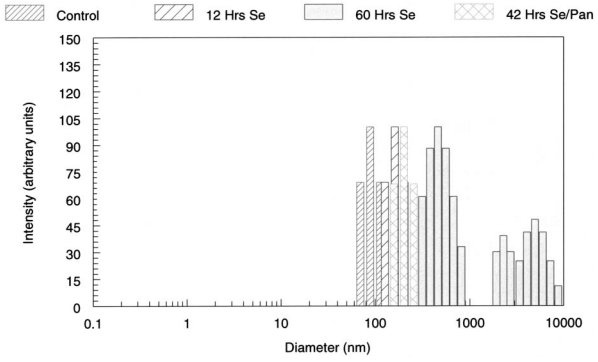

Fig. 20 Cataract treatment in rats. Analysis of particle size distribution with exponential sampling.

4.3.4 *Developing pharmacotherapy using SLS and DLS*

In the absence of a nonsurgical treatment, 50% of all blindness is due to cataracts. At present 34 million Americans over the age of 65 have cataracts. Foster predicts this figure to rise to 70 million by year 2030.[27] According to Kupfer,[28] "A delay in cataract formation of about 10 years would reduce the prevalence of visually disabling cataracts by about 45%." DLS can help achieve this goal by detecting cataracts at very early stages and by screening potential anticataract drugs for their efficacy.

Anticataract drug screening. The results of both preclinical and clinical tests of potential therapeutic agents indicate the need for more sensitive measures of protein aggregation and opacification *in vivo*. Studies in humans predict that DLS will be useful in testing anticataract drugs to inhibit or reverse the progression of cataract formation during longitudinal clinical trials.[11–13,29,30] Pantethine is a metabolically active, stable disulfide form of pantetheine and a derivative of pantothenic acid (vitamin B_5). It can be used as an anticataract drug, but the clinical trial of pantethine was inconclusive with respect to effectiveness.[29,31]

Recently Ansari et al.[32] using SLS and DLS demonstrated the efficacy of pantethine in very early stages (a few hours to a few days) of selenite-induced lens damage, well before the formation of a mature cataract in the selenite model.[33] In this study, SLS and DLS measurements were made on 33 animals (rats) aged 12 to 14 days at the time of selenite or pantethine injection. Pantethine treatment resulted in a substantial decrease in the dimensions of scattering centers in lens *in vivo* during the early stages of opacification prior to their detection with conventional ophthalmic instruments. An obvious opacity was not observed using a slit-lamp biomicroscope. Typical representative size distribution data are presented in Fig. 20 for a control, Se-treated (12 and 60 h post-treatment), and Se-pantethine-treated animal (42 h post-treatment) at a distance of about 2 mm from the anterior surface of the lens. The size distribution of scatterers in the control animal ranged from 60 to 80 nm in diameter. In the Se-treated animals, the TCF shows bimodal behavior with aggregates ranging in size from 400 to 800 nm and 3000 to 10,000 nm in diameter. The Se-pantethine-treated animal shows an aggregate size averaging around 200 nm. The experimental results clearly indicated that SLS and DLS were able to discern subtle molecular changes very early in cataract formation.[34] The results suggested that pantethine inhibits the initial aggregation process.

In conclusion, the results are encouraging. The future outlook for finding a medical cure for cataract seems optimistic when this effort is combined with advances in detection technology, understanding of fundamental processes, and the efforts in designing new anticataract drug formulations. This work is picking up momentum at Zigler's laboratory at the NEI/NIH.[35–37] In a recent pilot study, Congdon's group at Johns Hopkins University has shown that isoflavones can prevent or delay X-ray-associated cataract.[38] Also, Japanese investigators have demonstrated a delay in cataract in rats receiving miso (a soy-containing product) compared with control animals.[39]

4.4 *Vitreous and Diabetic Vitreopathy*

The vitreous is the least understood part of the eye since it remains transparent throughout life. Sebag discusses the role of vitreous in pathology and the technologies to image this transparent tissue in his review article in this issue. Ansari et al.[40] and Rovati et al.,[41] were the first to characterize vitreous structure with DLS and correlate the findings with diabetic retinopathy. In a DLS measurement, the vitreous body

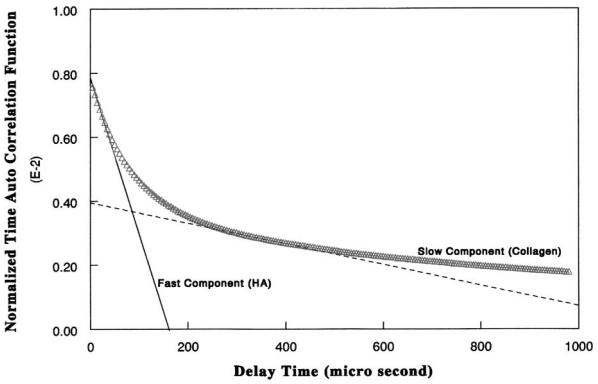

Fig. 21 Time relaxation of human vitreous.

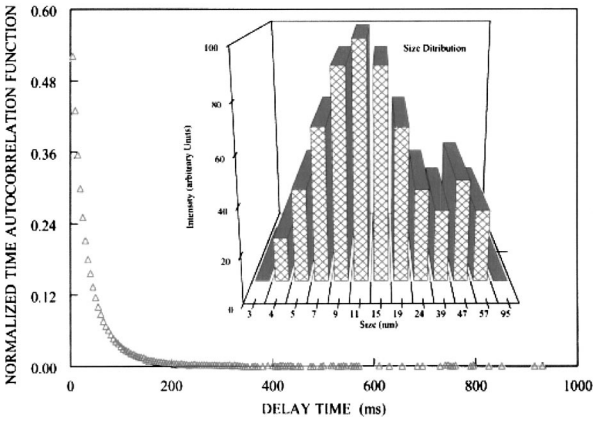

Fig. 22 Liquid bovine vitreous.

exhibits a two-exponential behavior consistent with its gel-like properties. Equation (1) can be rewritten in terms of a fast- and a slow-decaying component:

$$g^2(\tau) = I_{\mathrm{HA}} \exp(-D_{\mathrm{HA}} q^2 \tau) + I_{\mathrm{CL}} \exp(-D_{\mathrm{CL}} q^2 \tau), \quad (5)$$

where I_{HA} and I_{CL}, D_{HA} and D_{CL} are the scattering strengths and corresponding translational diffusion coefficients that are due to hyaluronan (HA) and collagen (CL) found in the vitreous gel. A typical measurement is shown in Fig. 21. The presence of a fast component in the TCF was confirmed by measuring liquid vitreous with DLS separately, as shown in Fig. 22. The average molecular weight (3.78×10^6 Dal) for the fast component obtained from DLS was consistent with the range (2 to 4.5×10^6) of values given by Balazs and Denlinger.[42] DLS becomes a powerful tool for studying the effects of diabetes on vitreous morphology, owing to the glycosylation of vitreous proteins, primarily collagen. Sebag discusses this in his article ''Seeing the Invisible'' in this issue.

5 Systemic and Other Diseases through the Eye

5.1 *Diabetes*

DLS can be used to detect early onset of diabetes through the transparent ocular lens. Chenault et al.[43] have indicated that cataracts are 1.6 times more common in diabetic patients than non-diabetics. The U.S. Food and Drug Administration (FDA) has a unique animal model for studying type II diabetes. *Psammomys obesus* (sand rat) is a wild rodent found in the desert areas of the Middle East and Africa. It develops mild to moderate obesity, hyperglycemia, and the complications of diabetes, such as cataracts and vision loss, when it consumes a high-calorie diet. In a recent study,[43] blood glucose levels, insulin, and glycohemoglobin values in this animal were correlated with histopathology, traditional ophthalmology assessments, and DLS measurements with a view toward developing a noninvasive means to detect early stages of eye damage that is due to diabetes mellitus. The control animals demonstrated no significant changes in particle size distributions. The study animals exhibited significant increases in the sizes of (crystallin) scattering centers and substantial shifts in the size distributions. No discernible difference between the control and study animals was observed by ophthalmic examination or by histology. The DLS results revealed subtle changes in the lens of the diabetic sand rats after only 2 months on the diabetogenic diet [Fig. 23(a)]. Conventional ophthalmic instrumentation did not detect these changes [Fig. 23(b)]. At the time of this writing, experiments using sand rats and SLS and DLS to screen some conventional and nonconventional drugs to control diabetes (hyperglycemia) and lens damage are under way at the FDA.

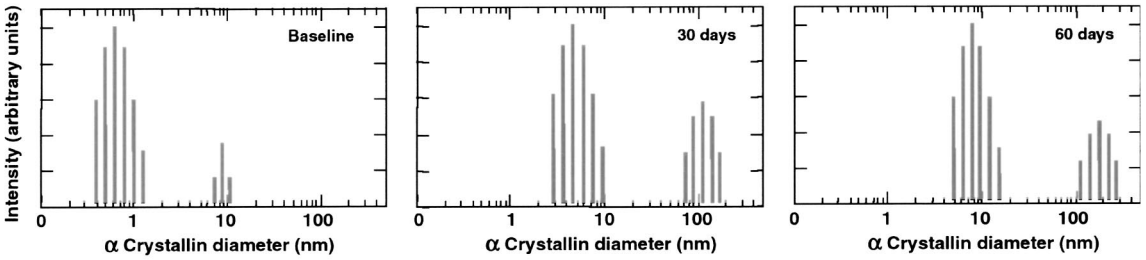

23 a

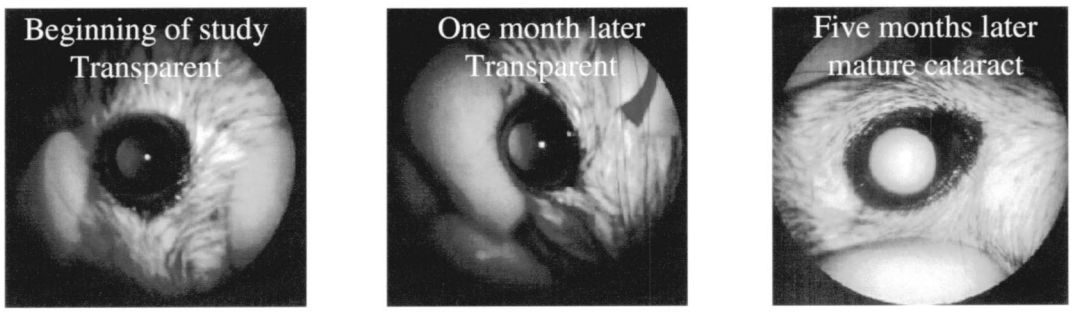

23 b

Fig. 23 Cataract damage that was due to diabetes in sand rats. (a) Particle size distribution as determined by DLS. (b) Slit-lamp photographs of eye. (Photos courtesy of Michelle Chenault, U.S. Food and Drug Administration.)

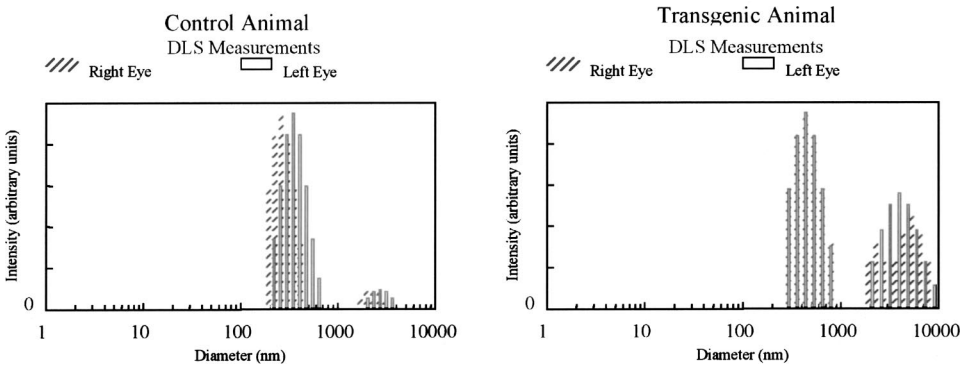

Fig. 24 Protein aggregation in the lens of transgenic mice.

5.2 *Alzheimer's Disease*

Like the ocular diseases described earlier, the incidence of Alzheimer's disease (AD) is expected to take on epidemic proportions in the next two to three decades. Can it be detected through the eye? This sounds like a radical idea because AD is a disease of the brain and not the eye. Frederikse et al.[44] at NEI/NIH were the first to demonstrate that Alzheimer's biology occurs in the lens. AD sufferers lose cognitive abilities and thus experience serious deterioration in the quality of life. In simplistic terms, amyloid proteins forming plaque on the brain tissue lead to development of AD. Currently, these amyloid deposits can only be studied under a microscope by looking at the brain tissue during autopsy. New *in vivo* experimental methods under investigation include positron emission tomography (PET) and magnetic resonance imaging (MRI), but their spatial and contrast resolution for very early detection of AD is questionable. Nevertheless these techniques are being used to follow treatment regimens in AD patients.

Recently, Frederikse provided evidence of amyloid protein structure in the lens and its association with cataractogenesis.[45] It was suggested by Goldstein et al.[46] that amyloid proteins may promote the aggregation of ocular proteins, linking the formation of supranuclear cataract in human lenses to AD. If this is true, then DLS can be used in the eye to detect early symptoms of AD. A proof-of-concept experiment was conducted *in vivo* by measuring protein aggregation in the lenses of transgenic mice. The results shown in Fig. 24 indicate enhanced aggregation in study animals as opposed to controls. The biochemical analysis conducted at autopsy and presented elsewhere supported the conclusions based on DLS.[46]

It seems that the ocular signs of AD are not confined to the lens. In a recent study by Janciauskiene et al.,[47] AD was linked to glaucoma and pseudoexfoliation syndrome by identifying Alzheimer's amyloids in the aqueous humor using electrophoresis followed by Western blotting. This opens up an opportunity for DLS to be used noninvasively in detailed studies of AD treatment using antiinflammatories, antioxidants, and hormone replacement therapies.

6 Bioastronautics (Celestial Teleophthalmology)

The absence of gravity in space affects human physiology. In some respects, the effect of space travel on the human body is similar to that of aging here on earth, e.g., osteoporosis and cataract. The development of cataract in astronauts is linked to radiation exposure even in low Earth-orbit missions, e.g., on board the space shuttle and space station orbiters.[2,3] This risk can be substantial if humans plan to travel to Mars.[48]

A head-mounted goggleslike device with a suite of noninvasive optical technologies is being developed in my laboratory at NASA to monitor the health of astronauts and ensure mission safety. DLS is one technique among several others to be integrated in this device, which may play an important role in monitoring ocular health remotely and noninvasively.[49] A prototype head-mounted DLS system is shown in Fig. 25.

7 Practical Considerations and Limitations

Several things can go wrong in a DLS experiment. Here I outline a few experimental tips to avoid disappointments and artifacts.

7.1 *Subject Variability*

The lens and vitreous, being transparent, do not have any visible markers. Therefore, in longitudinal studies, reproducibility in repeat patient visits remains a big concern. DLS instrumentation must have the ability to precisely control and sample the same location inside the tissue of interest. The eye movements must be controlled and the subject should remain well fixated during the DLS measurement cycle. In animal experiments, this is not much of a concern because animals

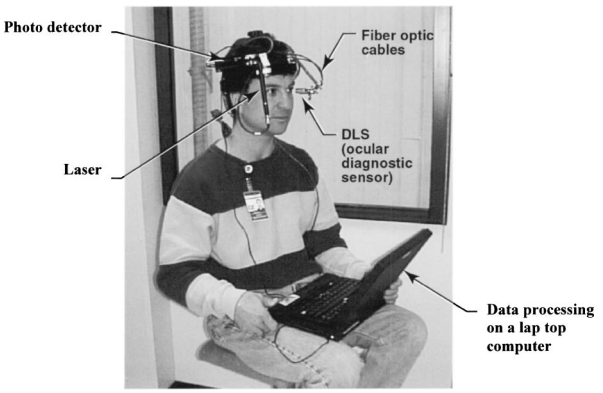

Fig. 25 Prototype of a head-mounted monitoring system for eye disease.

can be sedated. However, they should be closely watched since some animals roll their eyes while sedated.

7.2 *Safety*

In DLS ophthalmic applications, light from a laser source in the visible-infrared spectrum is used. Therefore the major safety concern is the amount of light exposure on the retina. To minimize the risks, the power levels must be low and the exposure time must be short to satisfy the safety requirements set by the American National Safety Institute. Current ophthalmic DLS instruments typically use a laser power of roughly 50 to 100 μW, with an exposure time of 5 to 10 s. This makes it several orders of magnitude lower and therefore safer for use in animals and humans. However, every DLS instrument has its own unique optical arrangement for launching and receiving light signals, alignment procedures, and maintaining coherence conditions inside the scattering volume. Therefore extra caution and care must be exercised in calculations for maximum permissible exposure (MPE) limits set by ANSI.

7.3 *Corneal Dryness and Body Temperature*

Drying of the cornea and the appearance of cold cataract produce artifacts, especially in animal measurements. Corneas should be constantly irrigated with saline solutions between the DLS measurements to avoid dehydration. In general, the body temperature of animals under anesthesia drops. This can cause cold-induced cataract, especially in mice and rats. This can be avoided by using a heating pad and keeping the body temperature constant around 37°C during the DLS experiments.

7.4 *Evaluation of Visible Abnormalities*

It is tempting to compare the DLS data, especially in clinical practice, with obvious ocular abnormalities. The techniques of SLS and DLS are only suitable for studies of very early ocular abnormalities. They are not suitable for studying visible or mature lens or corneal opacities. Such measurements will introduce artifacts that are due to multiple scattering of light, thus showing diffusion narrowing. The DLS data, especially in transparent lenses, when converted into particle size distributions, show quite nicely how a cataract is progressing. DLS can be used effectively in the determination of accurate particle sizes in water-based dispersions from transparent to extremely turbid (about 7 orders of magnitude higher than the turbidity of water) samples ranging in size from few nanometers to almost a micron. However, such analysis should be avoided in a cataractous eye because of unknown factors such as the changing viscosity. It is therefore acceptable to exploit the good dynamic range of DLS to follow a systematic trend as a marker for monitoring early ocular pathology, but due caution must be exercised in interpretating data when dealing with mild to advanced pathologies.

8 Concluding Remarks

The field of medicine in general and ophthalmology in particular has embraced the use of new technologies to make health care more effective. In the present climate, preventive medicine seems to be the direction of the future. Thus the early detection of ocular diseases long before the appearance of clinical symptoms to help find medical cures is the most desired goal. The new developments in SLS and DLS seem promising and indicate good potential to help achieve this goal. However, only time will tell if this ambitious goal of saving the gift of sight for millions of people can be accomplished.

Acknowledgments

I am indebted to many colleagues and collaborators with whom experiments reported in this review were conducted. These include Sam Zigler and Manuel Datiles of the National Eye Institute/National Institutes of Health in Bethesda, Maryland, for animal and clinical cataract studies; Luigi Rovati of the University of Modena in Italy for glaucoma studies; John Clark of the University of Washington in Seattle for pantethine treatment; Frank Giblin of Oakland University in Rochester, Michigan, for guinea pig HBO and rabbit X-ray studies; Michelle Chenault of the Food and Drug Administration in Rockville, Maryland, for studies on diabetic sand rats; Jerry Sebag of the Doheny Eye Institute in Los Angeles, California, for vitreopathy studies; Leo Chylack and Lee Goldstein of Harvard University in Boston for proof-of-concept Alzheimer's experiments; and Kwang Suh and Jim King of my laboratory for new instrument development. Support under National Aeronautics and Space Administration/National Institutes of Health and NASA-Food and Drug Administration interagency agreements on the development and use of DLS in ophthalmology, and funding from the John H. Glenn Biomedical Engineering Consortium for the bioastronautics research is greatly appreciated.

References

1. National Eye Institute (National Institutes of Health) and Prevent Blindness America, *Vision Problems in the U.S.: Prevalence of Adult Vision and Age-Related Eye Disease in America*, NEI/NIH, Bethesda, Md. (2002). Also available at www.usvisionproblems.org.
2. F. A. Cucinotta, F. K. Manuel, J. Jones, G. Iszard, J. Murrey, B. Djojonegro, and M. Wear, ''Space radiation and cataracts in astronauts,'' *Radiat. Res.* **156**(5), 460–466 (2001).
3. Z. N. Rastegar, P. Eckart, and M. Mertz, ''Radiation-induced cataract in astronauts and cosmonauts,'' *Graefe's Arch. Clin. Exp. Ophthalmol.* **240**(7), 543–547 (2002).
4. B. Chu, *Laser Light Scattering: Basic Principles and Practice*, Academic Press, New York (1991).
5. T. Tanaka and G. B. Benedek, ''Observation of protein diffusivity in intact human and bovine lenses with application to cataract,'' *Invest. Ophthalmol. Visual Sci.* **14**(6), 449–456 (1975).
6. S.-E. Bursell, P. C. Magnante, and L. T. Chylack, ''*In vivo* uses of quasi-elastic light scattering spectroscopy as a molecular probe in the anterior segment of the eye,'' in *Noninvasive Diagnostic Techniques in Ophthalmology*, B. R. Masters, Ed., pp. 342–365, Springer-Verlag, New York (1990).
7. R. S. Stock and W. H. Ray, *J. Polym. Sci.* **23**, 1393–1147 (1985).
8. H. S. Dhadwal, R. R. Ansari, and M. A. Dellavecchia, ''Coherent fiber optic sensor for early detection of cataractogenesis in a human eye lens,'' *Opt. Eng.* **32**(2), 233–238 (1993).
9. L. Rovati, F. Fankhauser II, and J. Rick, ''Design and performance of a new ophthalmic instrument for dynamic light scattering in the human eye,'' *Rev. Sci. Instrum.* **67**(7), 2615–2620 (1996).
10. R. R. Ansari, K. I. Suh, A. Arabshahi, W. W. Wilson, T. L. Bray, and L. J. DeLucas, ''A fiber optic probe for monitoring protein aggregation, nucleation and crystallization,'' *J. Cryst. Growth* **168**, 216–226 (1996).
11. G. M. Thurston, D. L. Hayden, P. Burrows, J. I. Clark, V. G. Taret, J. Kandel, M. Courogen, J. A. Peetermans, M. S. Bowen, D. Miller, K. M. Sullivan, R. Storb, H. Stern, and G. B. Benedek, ''Light scattering

from the aging human lens *in vivo*,'' *Curr. Eye Res.* **16**(3), 197–207 (1997).
12. H. Dhadwal and J. Wittpen, ''*In vivo* dynamic light scattering characterization of the human lens: cataract index,'' *Curr. Eye Res.* **20**(6), 502–510 (2000).
13. M. B. Datiles III, R. R. Ansari, and G. F. Reed, ''A clinical study of the human lens with a dynamic light scattering device,'' *Exp. Eye Res.* **74**(1), 93–102 (2002).
14. M. B. Datiles III, B. V. Magno, and V. Freidlin, ''Study of nuclear cataract progression using the National Eye Institute Scheimpflug system,'' *Br. J. Ophthamol.* **79**, 527–534 (1995).
15. C. W. Oyster, *The Human Eye Structure and Function*, Sinauer Associates (1999).
16. J. A. Castoro, A. Adriel, and F. A. Bettelheim, ''Water gradients across bovine cornea,'' *Invest. Ophthalmol. Visual Sci.* **29**(6), 963–968 (1988).
17. M. Lipner, ''Keeping LASIK patients out of dry-dock,'' *Eye World* **7**(1), 21–22 (2002).
18. S. D. McLeod, ''Beyond Snellen acuity: the assessment of visual function after refractive surgery,'' *Arch. Ophthalmol. (Chicago)* **119**, 1371–1373 (2001).
19. L. B. Sabbagh, ''Dynamic light scattering focuses on the cornea,'' *Rev. Ref. Surg.* **3**(2), 28–31 (2002).
20. R. R. Ansari, A. K. Misra, A. B. Leung, J. F. King, and M. B. Datiles III, ''Noninvasive evaluation of corneal abnormalities using static and dynamic light scattering,'' *Proc. SPIE* **4611**, 220–229 (2002).
21. L. Pollonini, L. Rovati, and R. R. Ansari, ''Dynamic light scattering and natural fluorescence measurements in healthy and pathological ocular tissues,'' *Proc. SPIE* **4611**, 213–219 (2002).
22. M. B. Datiles and R. R. Ansari ''Clinical evaluation of cataracts,'' in *Duane's Clinical Ophthalmology, 2004 Edn.*, W. Tasman and E. Jaeger, Eds., Chap. 73B, Lippincott, Philadelphia, Pa (2003).
23. R. R. Ansari, K. I. Suh, S. J. Tumminia, P. Russell, and J. S. Zigler, Jr., ''*In-vivo* cataractograms using a compact backscatter dynamic light-scattering (DLS) probe,'' *Proc. SPIE* **3192**, 202–210 (1997).
24. S. J. Tumminia, G. J. Jonak, Y.-S. Focht, E. Cheng, and P. Russell, ''Cataractogenesis in transgenic mice containing the HIV-1 protease linked to the lens αA-crystallin promoter,'' *J. Biol. Chem.* **271**(1), 425–431 (1996).
25. F. A. Bettelheim, F. F. Zeng, Y. Bia, S. J. Tumminia, and P. Russell, ''Lens hydration in transgenic mice containing HIV-1 protease linked to the lens αA-crystallin promoter,'' *Arch. Biochem. Biophys.* **324**(2), 223–227 (1995).
26. American Academy of Ophthalmology, *Basic and Clinical Science Course 1989–1990*, Sec. 8, pp. 107–108, American Academy of Ophthalmology, San Francisco (1989).
27. A. Foster, ''Cataract- a global perspective: output, outcome and outlay,'' *Eye* **3**, 449–453 (1999).
28. C. Kupfer, ''The conquest of cataract: a global challenge,'' *Trans. Ophthalmol. Soc. U. K.* **104**, 1 (1984).
29. G. B. Benedek, J. Pande, G. M. Thurston, and J. I. Clark, ''Theoretical and experimental basis for the inhibition of cataract,'' *Prog. Retin. Eye Res.* **18**, 391–402 (1999).
30. G. M. Thurston, D. L. Hayden, P. Burrows, J. I. Clark, V. G. Taret, J. Kandel, M. Courogen, J. A. Peetermans, M. S. Bowen, D. Miller, K. M. Sullivan, R. Storb, H. Stern, and G. B. Benedek, ''Evidence for increased interprotein association as a function of age in the living human lens using quasielastic light scattering,'' *Curr. Eye Res.* **16**, 197–207 (1977).
31. J. J. Harding, *Drugs Aging* **18**(7), 473–486 (2001).
32. R. R. Ansari, J. I. Clark, J. F. King, and T. Seeberger, ''Early detection of cataracts and response to therapy with non-invasive static and dynamic light scattering,'' *Proc. SPIE* **4951**, 168–175 (2003).
33. J. I. Clark, J. C. Livesey, and J. E. Steele, ''Delay or inhibition of rat lens opacification using pantethine and WR-77913,'' *Exp. Eye Res.* **62**, 75–85 (1996).
34. J. L. Clark, J. K. King, T. M. Seeberger, and R. R. Ansari, ''Non-Invasive DLS detects the earliest stages of cataract and inhibition of lens opacification by pantethine *in vivo*,'' *Invest. Ophthalmol. Visual Sci.* **44**, 3482 (2003).
35. F. A. Bettelheim, R. R. Ansari, Q. F. Cheng, and J. S. Zigler, ''The mode of chaperoning of dithiothreitol-denatured α lactalbumin by α crystallin,'' *Biochem. Biophys. Res. Commun.* **261**, 292–297 (1999).
36. J. S. Zigler et al., Hydroxylamine compositions for the prevention or retardation of cataracts, U.S. Patent 6,001,853, Dec. 14, 1999.
37. J. S. Zigler, C. Qin, J. S. Tumminia et al., ''Prevention of cataractous changes in cultured rat lenses by the hydroxylamine of Tempol (Tempol-H),'' *Invest. Ophthalmol. Visual Sci.* **37**(3), 970–970 (1996).
38. C. Nduagubal, N. Congdon, M. Mahmoud, M. Daly, H. Lai, and E. deJuan, ''Dietary genistein is protective against X-ray cataract in the rat,'' *Invest. Ophthalmol. Visual Sci.* **44**, 4322 (2003).
39. T. Gotoh, K. Yamada, A. Ito, H. Yin, T. Kataoka, and K. Dohi, ''Chemoprevention of *N*-nitroso-*N*-methylurea-induced rat mammary cancer by miso and tamoxifen, alone and in combination,'' *J. Intern Med.* **89**, 487–495 (1998).
40. R. R. Ansari, K. S. Suh, S. Dunker, N. Kitaya, and J. Sebag, ''Quantitative molecular characterization of bovine vitreous and lens with non-invasive dynamic light scattering,'' *Eye Res.* **73**, 859–866 (2001).
41. L. Rovati, F. Fankhauser II, F. Docchio, and J. Van Best, ''Diabetic retinopathy assessed by dynamic light scattering and corneal autofluorescence,'' *J. Biomed. Opt.* **3**(3), 357–363 (1998).
42. R. E. A. Balazs and J. L. Denlinger, ''The vitreous,'' in *The Eye*, 3rd ed., Vol. IA, pp. 533–589, Academic Press, New York (1984).
43. V. M. Chenault, M. N. Ediger, and R. R. Ansari, ''*In vivo* assessment of diabetic lenses using dynamic light scattering,'' *Diab. Tech. Therap.* **4**(5), 651–659 (2002).
44. P. H. Frederikse, D. Garland, and J. S. Zigler et al., ''Oxidative stress increases production of beta-amyloid precursor protein and beta-amyloid (A beta) in mammalian lenses, and A beta has toxic effects on lens epithelial cells,'' *J. Biol. Chem.* **271**(17), 10169–10174 (1996).
45. P. H. Frederikse, ''Amyloid-like protein structure in mammalian ocular lenses,'' *Curr. Eye Res.* **20**(6), 462–468 (2000).
46. L. Goldstein, J. Muffat, R. Cherny, K. Faget, J. Coccia, F. Fraser, C. Masters, R. Tanzi, L. Chylack, Jr., and A. Bush, ''αBeta peptides in human and amyloyd-bering transgenic mouse lenses: implications for alzheimer's disease and cataracts,'' *Invest. Ophthalmol. Visual Sci.* **42**(4), ARVO abstract 1614 (2001).
47. S. Janciauskiene and T. Krakau, ''Alzheimer's peptide and serine proteinase inhibitors in glaucoma and exfoliation syndrome,'' *Doc. Ophthalmol.* **106**(3), 215–223 (2003).
48. R. R. Ansari, L. Rovati, and J. Sebag, ''Non-invasive and remote detection of cataracts during space exploration with dynamic light scattering,'' *Proc. SPIE* **4245**, 129–134 (2001).
49. R. R. Ansari, L. Rovati, and J. Sebag, ''Celestial and terrestrial teleophthalmology: a health monitoring helmet for astronauts/cosmonauts and general public use,'' *Proc. SPIE* **4245**, 177–185 (2001).